

Evaluation and Field Calibration of a Low-Cost Ozone Monitor at a Regulatory Urban Monitoring Station

Mauro Masiol,¹ Stefania Squizzato,¹ David Chalupa,² David Q. Rich,^{1,2} Philip K. Hopke,^{1,3,†}

¹ *Department of Public Health Sciences, University of Rochester Medical Center, Rochester, NY 14642*

² *Department of Environmental Medicine, University of Rochester Medical Center, Rochester, NY 14642, United States*

³ *Center for Air Resources Engineering and Science, Clarkson University, Potsdam, NY 13699*

ABSTRACT

The performance of a low cost ozone monitor (Aeroqual Series 500 portable gas monitors coupled with a metal oxide sensor for ozone; model OZL) was assessed under field conditions. Ten ozone monitors were initially calibrated in clean-air laboratory conditions and tested at controlled ozone concentrations of 5 to 100 ppb. Results showed good linearity and fast response with respect to a conventional research-grade ozone monitor. One monitor was then co-located at a regulatory air quality monitoring station that uses a U.S. federal equivalent method (FEM) ozone analyzer. Raw data from the Aeroqual monitor collected over 4 months (June-October) at a 10-minute time-resolution, showed good agreement ($r^2=0.83$) with the FEM values but with an overestimation of ~12%. Data were averaged to different time resolutions; 1 h time averaged concentrations showed the best fit with the FEM results ($r^2=0.87$). An analysis of the ratio of FEM/monitor concentrations against chemical and meteorological variables suggested the potential of interferences due to temperature, relative humidity, nitrogen oxides, and volatile organic compounds. Three correction models using temperature, humidity, and nitrogen dioxide (NO₂) were then tested to better relate the monitor concentrations to the FEM values. Temperature and humidity are two variables commonly available (or easily measurable) at sampling sites. The model (#3) that added NO₂ did not provide a substantial improvement in the fit. Thus, the proposed models with only temperature and humidity can be easily adopted and adapted by any user. The corrected data explained up to 91% of the variance and showed statistically significant improvement of the goodness of fits as well as decreased influence of the interfering variables on the diurnal and weekly patterns. The correction models were also able to lower the effect of seasonal temperature changes, allowing the use of the monitors over long-term sampling campaigns. This study demonstrated that the Aeroqual ozone monitors can return “FEM-like” concentrations after appropriate corrections. Therefore, data provided by a network of monitors could determine the intra-urban spatial variations in ozone concentrations. These results suggest that these monitors could provide more accurate human exposure assessments and thereby reduce exposure misclassification and its resulting bias in epidemiological studies.

Keywords: Semiconductor gas sensor, tropospheric ozone, urban air pollution, air pollution exposure

[†] Author to whom correspondences should be addressed. Email: phopke@clarkson.edu

41 1. INTRODUCTION

42 Tropospheric ozone (O_3) is a greenhouse gas and an air pollutant (Stevenson *et al.*, 2013;
43 Cooper *et al.*, 2014; Monks *et al.*, 2015) known to be harmful to human health (Jerrett *et al.*,
44 2009; Bell *et al.*, 2014; Turner *et al.*, 2016) and ecosystems (Fowler *et al.*, 2009; Ainsworth *et al.*,
45 2012). In U.S., the National Ambient Air Quality Standards (NAAQS) set the limit values for the
46 protection of public health (primary standard) and public welfare (secondary standard) of six
47 principal “criteria” air pollutants, including ozone. Concentrations of ozone are measured using
48 federal “reference” or “equivalent” methods (FRM and FEM, respectively) in accordance with
49 Code of Federal Regulations (40 CFR Part 53; USEPA, 2017). Compliance with NAAQS within
50 major cities is routinely evaluated at one or a few static urban stations. The spatial coverage of
51 monitoring networks is therefore insufficient to capture the spatial variability due to the effect of
52 major roadways, complex terrain, urban heat island effects, and the locations and strengths of
53 local sources of ozone precursors (i.e. nitrogen oxides ($NO_x=NO+NO_2$), carbon monoxide (CO),
54 and reactive volatile organic compounds (VOCs) of biogenic and anthropogenic origin.

55 Recent advances in micro-scale technology have made available inexpensive and reliable
56 sensors and low power electronic circuits and memory, allowing the development of a series of
57 low-cost (and relatively low-cost) air quality monitors. These devices are much less expensive
58 than research-grade instruments, have low power requirements, and are physically smaller and
59 lighter (mostly portable). Although the use of this technology increases the potential spatial
60 resolution of monitoring networks, current monitors are not designed to meet rigid performance
61 standards and generate less accurate data than research-grade instruments (White *et al.*, 2012;
62 Snyder *et al.*, 2013; Kumar *et al.*, 2015). This limitation can be addressed by careful calibration
63 of the units and post-processing of the raw data before they can be used for scientific purposes.

64 A cost-efficient ozone monitor using gas-sensitive semiconducting oxide (GSS)
65 technology was co-located over 4 months to a routine air quality monitoring station in a medium-
66 sized city of the Northeast U.S. (Rochester, NY). Ozone concentrations were compared with
67 those measured by a FEM instrument and an extensive series of additional air pollutants and
68 weather data measured with scientific-grade or conventional instruments. A series of
69 chemometric approaches were adopted to (i) calibrate the monitor, (ii) evaluate the effects and
70 interferences with other measured air pollutant species under field conditions, (iii) correct the
71 data for interferences to return unbiased concentrations as similar as possible to the reference

72 method (FEM), and (iv) discuss strengths and limits of using GSS technology for scientific
73 purposes.

74

75 **2. MATERIALS AND METHODS**

76 **2.1 Study area**

77 Rochester, NY, (~210,000 inhabitants, 2010 Census) is the center of the Greater
78 Rochester metropolitan area (~1.1 million inhabitants) and lies on the southern shore of Lake
79 Ontario. It is typical of NE U.S. moderate sized, urban areas. Road traffic is a major source of
80 CO, NO_x, and PM_{2.5} (Figure S1 in the supplemental information file). This study was performed
81 at the regulatory air quality station in Rochester (ROC; USEPA 36-055-1007) operated by the
82 New York State Department of Environmental Conservation (NYSDEC). The site lies ~300 m
83 from the intersection of two major highways with an average traffic of ~ 230,000 vehicles/day
84 (Figure S1). Diesel-powered trains operate on a mainline track affect the site with a switching
85 yard about 1.5 km NW of the site. Regional advection of polluted air masses from Buffalo (NY),
86 the Ohio River Valley, eastern coast of the U.S. and occasionally from Toronto (ON) also affect
87 local air quality (Emami *et al.*, 2018).

88

89 **2.2 Experimental**

90 Ten Aeroqual (Auckland, New Zealand) Series 500 portable gas monitors coupled with
91 metal oxide (WO₃) GSS sensors for ozone (model OZL) were purchased in April 2017.
92 Technical details of these monitors are discussed elsewhere (Aliwell *et al.*, 2001; Williams *et al.*,
93 2009; 2013) and summarized in Table S1. The sensor operates in the 0 to 0.5 ppm O₃
94 concentration range and has a minimum detection limit (MDL) of 0.001 ppm with an accuracy of
95 0.008 ppm over the 0 to 0.01 ppm range and $\leq \pm 10\%$ for the rest of the range. Preliminary tests of
96 this type of sensor under field conditions reported promising results. Bart *et al* (2014) reported
97 that differences (GSS-reference instrument) in hourly average ozone concentrations were
98 normally distributed with a mean = -0.001 ppm and standard deviation = 0.006 ppm. Lin *et al.*
99 (2015) reported a high coefficient of determination ($r^2=0.91$) with values measured with a
100 reference ultraviolet absorption O₃ analyzer.

101 In this study, one monitor was placed on the roof of the NYSDEC ROC station (Figure
102 S2) in a waterproof plastic-fiberglass enclosure with two 90° bend inlets (2 cm in diameter) and a

103 USB-powered fan (4500 RPM) to promote air throughput (Figure S2). A single layer of
104 screening was placed on each inlet to prevent coarse debris and insects from entering the
105 enclosure. A low-cost PM monitor (Speck, Airviz Inc., PA) that also has a temperature sensor
106 was installed in a similar box side-by-side to the ozone monitor (Zikova *et al.*, 2017). This latter
107 monitor was used to measure the air temperature inside the enclosures, i.e. monitoring the
108 potential diurnal temperature from increasing solar irradiance heating. The monitor was powered
109 with a 12 V DC power supply, but also had a Li-ion 2700 mA h⁻¹ battery to eliminate the effects
110 of short-term power outages (up to ~8 h). The sampling campaign extended over 4 months (June
111 9 to October 11, 2017). Data were collected with a time resolution of 10 minutes. Periodic
112 checks of the fan operation, downloads of the data, and cleaning of the inlets were performed
113 throughout the sampling campaign.

114

115 **2.3 Air quality and weather variables**

116 Concentrations of CO, NO_x, total reactive nitrogen (NO_y), SO₂, O₃, PM₁₀ and PM_{2.5} were
117 routinely measured by NYS DEC in accordance with federally mandated methods at a 1-minute
118 time resolution. NO₂ was estimated as NO_x-NO. PM_{2.5}-bound equivalent black carbon (BC) was
119 measured using an aethalometer (Magee model AE-22). Particle number concentrations (PNC)
120 were measured with a scanning mobility particle spectrometer (SMPS) at 5 min resolution time.
121 The number concentrations were split into three ranges roughly representative of nucleation
122 (NUC: 11-50 nm), Aitken nuclei (AIT: 50-100 nm) and accumulation (ACC: 100-470 nm)
123 particles. Details are reported in Table S2. FEM ozone was detected with a Teledyne API T400
124 photometric analyzer based on ultraviolet absorption (automated equivalent method EQOA-
125 0992-087) (USEPA, 2017; NYSDEC, 2017). The FEM analyzer is regularly calibrated weekly to
126 a secondary transfer standard reference, a photometric O₃ calibrator/analyzer (Teledyne,
127 Advanced Pollution Instrumentation, model API 703E). This secondary reference standard is
128 regularly checked (bi-annually) with a NIST primary reference O₃ standard in Albany, NY, as
129 per the Ozone Transfer Standard Guidance Document 10/2013 (USEPA, 2013).

130 Meteorological data (air temperature (°C), relative humidity (RH, %), barometric
131 pressure (hPa), wind speed (m s⁻¹) and direction) were measured at a 1-h time resolution. Since
132 ROC wind data are potentially affected by surrounding building and street canyon effects, the
133 same set of weather variables (including precipitation) measured at the Greater Rochester

134 International Airport (KROC) at 1-h intervals were retrieved from the NOAA National Climatic
135 Data Center. Relative humidity values were estimated using data provided by the dense network
136 of personal weather stations across the Monroe County. The reliability of data provided by these
137 personal stations was carefully evaluated and checked with the help of the modeled humidity
138 data provided by the NOAA-NCEP North American Regional Reanalysis (NARR) model at 32
139 km spatial resolution (every 3 hours).

140 Additional 3-hour time-resolved meteorological variables estimated by meteorological
141 models were retrieved from the NOAA' National Centers for Environmental Prediction (NCEP)
142 North American Regional Reanalysis (NARR; Mesinger *et al.*, 2006). These results included
143 downward long- and short-wave radiation fluxes ($W m^{-2}$), upward long- and short-wave radiation
144 fluxes ($W m^{-2}$), planetary boundary layer height (m), and forecast total cloud cover (%). The
145 NARR spatial resolution is ~ 32 km. Final data were calculated as averages within a circular
146 buffer of radius 32 km from the sampling station coordinates.

147

148 **2.4 Data analyses**

149 Air pollutant data were matched with wind data to investigate the potential local source
150 locations by using polar-plots and polar-annuli. Briefly, polar-plots present the statistics of
151 variables by mapping wind speed and direction as a continuous surface with the surfaces
152 calculated using smoothing techniques (Carslaw *et al.*, 2006). Polar-annuli allow mapping wind
153 direction and time of day as continuous surfaces and can present conditional bivariate probability
154 function (CBPF; Uria-Tellaetxe and Carslaw, 2014) or Pearson' correlations between pair of
155 variables (Grange *et al.*, 2016). The linear trends of the FEM/Aeroqual ratios throughout the
156 sampling campaign were assessed with the Theil-Sen nonparametric estimator of slope (Theil,
157 1950; Sen, 1968) that assumes monotonic linear trends and is robust against outliers. Slopes were
158 computed over daily-averaged data (calculated when at least 75% of data are available).

159

160 **3. RESULTS AND DISCUSSION**

161 **3.1 Initial laboratory calibration**

162 Although the sensors used in this study were new with factory calibration certificates, the 10
163 monitors were calibrated under laboratory conditions prior to the co-location campaign.

164 Historical data measured in Rochester (Emami *et al.*, 2018; Squizzato *et al.*, submitted) indicate

165 that summertime hourly ozone peaks never exceeded 100 ppb after 2012. Consequently, the span
166 was calibrated at 100 ppb through a 24 h co-location with an ultraviolet photometric ozone
167 analyzer (Model 49i, Thermo Scientific, Franklin, MA; automated equivalent method EQOA-
168 0880-047). This laboratory reference instrument was calibrated using the same secondary API
169 703 used to calibrate the FEM analyzer at ROC. Ozone was generated in a clean-air room (trace
170 NO and NO₂; and PNC <100 particles/cm³) with a Corona spark discharge (model V5-0, Ozone
171 Research and Equipment Corp., Phoenix, AZ) coupled with an ozone calibrator (model 1008-PC,
172 Dasibi Environmental Corp., Glendale, CA). After the span calibration, the monitors were
173 operated overnight with laboratory clean-air O₃ concentrations (<5 ppb). They were checked
174 again the following day at 50 and 100 ppb. Very good agreement was found (mean ± std.
175 deviation of reference instrument/Aeroqual ratio at 100 ppb= 0.99 ± 0.02). The linearity of the
176 Aeroqual monitor responses was again tested at the end of the campaign with the same
177 laboratory procedure for >2 hours and 3 concentration steps (5, 50 and 100 ppb). Results
178 indicated very good linear response to the varying ozone concentrations (r²=0.99 using 132
179 readings). However, there were small shifts in the slopes of the response curves from the initial
180 calibration.

181

182 **3.2 Field co-location**

183 One monitor was co-located at the ROC site with the FEM monitor. Figures S3 and S4 show the
184 boxplots and diurnal profiles of variables measured at ROC. The ambient air temperature
185 recorded during the co-location study (average 20.8°C, range 5-35°C) was within the operating
186 range of GSS sensors (0-40°C) as well as the temperature inside the enclosure (average 21.9°C,
187 range from 0 to 38°C). However, ~19% of data were collected under RH levels exceeding the
188 operating range (>90%), mostly occurring overnight (1-5 am; Figure S5).

189 During the co-location study, the average ozone concentrations measured with FEM and
190 Aeroqual were 31 and 34 ppb, respectively. The average FEM/Aeroqual ratio was 0.88. Since the
191 monitor was initially calibrated under clean air conditions, the ~12% overestimation is an
192 indication of the interfering substances that affect the GSS sensor sensitivity under field
193 conditions. Aeroqual overestimation (lower ratios) was more frequent during overnight periods
194 (Figure S4), particularly in the early morning (5-7 am local time), when lowest air temperature

195 and highest RH were observed. A fast increase of FEM/Aeroqual ratio occurred during 7-10 am,
196 concurrent to the morning rush hours for road traffic (peaks of nitrogen oxides, CO and BC;
197 Figure S4), and increasing solar irradiance.

198 Pearson product-moment correlation coefficients were calculated among the available
199 variables to explore the linear relationships at different time resolutions. Results are arranged as
200 correlograms in Figure S6. The FEM/Aeroqual ratio is moderately ($r > 0.6$) positively correlated
201 with FEM ozone concentration, temperature (both ambient air and enclosure) and weakly to
202 moderately ($0.4 < |r| < 0.6$) negatively correlated with RH at both 10 min and 1 h time-resolutions.
203 The positive correlation with temperature reflects the known decrease in the GSS sensors
204 sensitivity with increased temperature. Since the sensitivity of the monitor was highly linear
205 under lab conditions ($R^2 = 0.99$ over the 5-100 ppb concentration range), the correlation of the
206 ratio with the FEM ozone concentrations likely reflects the correlations between O_3 and air
207 temperature ($r = 0.73$ and 0.74 , for 10-min and 1-h average data, see Figure S6) rather than a non-
208 linear response of GSS sensors. The potential interference of other atmospheric oxidants
209 (possibly radicals) cannot be disregarded. The moderate correlation with RH, but not absolute
210 humidity, is another indication of the temperature effects on the sensor sensitivity. The
211 sensitivity of GSS to ambient water vapor was previously reported by Bart et al. (2014).
212 However, this study found a small systematic error associated with variation of atmospheric
213 relative humidity.

214 GSS sensors are sensitive to several gaseous species, including NO_2 and VOCs. During
215 the time of this study, nitrogen oxides were largely emitted by road traffic (Figure S3) along with
216 anthropogenic VOCs (with the additional emissions from building and domestic heating in the
217 colder period at the end of the study period). In addition, highly reactive biogenic VOCs
218 (isoprene and terpenes) are present, particularly during the summer (Palmer *et al.*, 2003;
219 Sindelarova *et al.*, 2014). While NO_2 leads to positive artifacts, VOCs (e.g., butane, heptane,
220 propane, toluene, and particularly alkenes) may cause a reduction in the GSS sensitivity
221 (Aeroqual, 2018). The VOCs are reactants that participate in ozone formation and react with
222 oxidants in many atmospheric processes (Monks, 2005; Seinfeld and Pandis, 2016; Monks *et al.*,
223 2015). Unfortunately, VOCs are not measured hourly at the station. Therefore, their effects on
224 the sensor cannot be evaluated directly. Since Lin *et al.* (2015) reported a limited effect of NO_2
225 on GSS sensors, the poor ($0.3 < |r| < 0.4$) negative correlations with NO - NO_2 - NO_y likely reflect the

226 simultaneous effects of multiple species (mostly VOCs) rather than the sole interference of
227 nitrogen oxides.

228 The Theil-Sen nonparametric estimator of slope was computed on the daily-averaged
229 FEM/Aeroqual ratios to detect the presence of significant slopes in the data that may be
230 indicative of potential instrumental sensitivity drift. Figure S7a shows a statistically significant
231 ($p < 0.001$) negative slope (-0.016/week; 95% confidence interval: -0.021 to -0.011) indicating an
232 increase in the GSS sensitivity throughout the sampling campaign. This result may be biased by
233 air temperatures variations from June to October that showed a similar negative trend.

234

235 **3.3 Calibration using FEM data**

236 The linear response of the GSS sensor to ozone concentrations over the 5 to 100 ppb
237 range, assessed under laboratory conditions indicated that a simple linear regression between
238 concentrations measured by the monitor (dependent variable) and the FEM instrument
239 (independent variable) is likely to be sufficient for calibration. Figure 1a-e shows results from
240 the linear regression models computed from 10 min time resolution data as well as from
241 increasingly longer time averaged data (from 20 minutes to 1 day). Figure 1f presents the
242 changes in the coefficient of determination and regression coefficients at the various time
243 resolutions and the relative cross-correlations over 24 h lags. The results indicate that the
244 Aeroqual and FEM have a similar response rate to ozone concentrations (cross-correlations
245 peaked at 0 lags using 10 min time intervals and over all the time resolutions). The Aeroqual data
246 were able to explain between 74% and 87% of variability of FEM ozone, with a maximum r^2 for
247 the 1-h interval data. Regression slopes are also higher for 30 min to 2 h average data and have
248 smaller intercepts.

249 Since the 1-h data provided the best fit with the FEM data and this time resolution is
250 commonly adopted by routine regulatory monitoring networks, the calibration of Aeroqual was
251 calculated for the 1-h time-averaged data. This procedure returned FEM-calibrated data, i.e.
252 Aeroqual data with null intercept, unitary slope and explaining 87% of the original variance
253 ($r^2 = 0.87$). A better estimation of the average model prediction errors was assessed by the root-
254 mean-square error (RMSE) and mean absolute error (MAE), two measures of the average
255 differences (in ppb) between values measured by FEM and predicted by the linear model.
256 Results show an average prediction error of 4 ppb (MAE) and 5 ppb (RMSE). The calibration

257 was able to approximate the average diel and weekly patterns in the FEM data (Figure 2).
258 However, the calibrated data still had a general underestimation during early mornings and on
259 Sundays and an overestimation during the afternoon and on week days. The Theil-Sen slope
260 analysis (Figure S7b) found a lower negative slope of the FEM/Aeroqual ratios (-0.011/week;
261 95% confidence interval: -0.02 to 0.002). However, the trend was still statistically significant at
262 $p < 0.05$.

264 3.4 Presence of an edge

265 Figure 1c also shows the presence of an edge splitting record with unusually high
266 FEM/Aeroqual ratios ($n=64$, 2.3% of total collected data with 1-h time resolution). Figure S8a
267 highlights the edge and displays the occurrence of these events by day and by hour of day. Most
268 of the “high-ratio” events (HRE) occurred at the beginning of the sampling campaign (middle of
269 June), a few occurrences (4 records) on July 6th. No events were detected between August and
270 October (Figure S8b). All HRE occurred during daytime, peaking around noon (Figure S8c).
271 Figure S8 also shows that the regression r^2 increases from 0.87 to 0.9 by excluding these HRE
272 observations.

273 Figure S9 shows the differences between the “non-edge” data and HRE for selected
274 variables with Kruskal–Wallis one-way analysis of variance tests. Although these tests indicated
275 statistically significant differences ($p < 0.05$) between the HRE and normal measurements, these
276 differences were not able to fully explain the presence of the edge, i.e. HRE variability is within
277 the variance of the “non-edge” observations. Wind directionality analysis was performed using
278 polar-plots (Figure S10) and polar-annuli (Figure S11) to investigate possible interferences from
279 local sources or peculiar wind regimes causing the HREs. The highest averages and the highest
280 CBPF probabilities for the FEM/Aeroqual ratio were observed for high winds (speed > 6 m/s)
281 blowing from SW during the daytime with similar results for the FEM O₃ concentrations. No
282 unusual patterns were observed with respect to the correlations of FEM/Aeroqual ratio with FEM
283 O₃, air temperature, RH, or downward shortwave irradiation flux (Figure S12). However, careful
284 examination of the HRE occurrences in the bivariate plot of enclosure temperature vs. RH
285 (Figure S13) clearly shows that the HREs occurred when there were high temperatures and low
286 RH. The reason(s) for this combination driving these unusual values is not understood.

287

288 3.5 Corrections

289 The calibration with FEM ozone through linear regression was sufficient to achieve a
290 reasonable goodness of fit. However, the presence of the HREs potentially affected by
291 temperature and humidity (Figure S13) could be accounted for to better approximate Aeroqual
292 data to FEM values. A series of subsequent approaches were tested to correct the data for
293 temperature and RH. The choice of the best method depends on several factors: (i) atmospheric
294 species having effects on the GSS sensitivity are not always measured where the monitors are
295 deployed; (ii) the interplay of interfering species may cause different artifacts (positive, negative,
296 or mixed) that are difficult to separate and adjust for; (iii) the effect of the interfering effects may
297 not be linear; and (iv) there can be multicollinearity between independent variables that may
298 obscure the statistical significance of the models.

299 The first model (model 1) developed linear relationships of the Aeroqual O₃ with FEM
300 O₃, enclosure temperature, and RH. The results are reported in Table 1 and Figure 2b. They
301 show an overall improvement in the goodness of fit from the initial calibration results. The
302 adjusted r^2 improved to 0.89, the partial F-test indicated statistically significant improvement of
303 the fit at $p < 0.001$, RMSE and MAE decreased, and all the independent variables were highly
304 statistically significant ($p < 0.001$) in the model. Model 1 also provided a better fit of the daily
305 averages (RMSE=0.4) but not the weekly pattern and resulted in a further decrease in the Theil-
306 Sen slope (Figure S7).

307 Figure S14 shows the relationships of selected variables against the differences between
308 the concentrations measured by the Aeroqual monitor and the FEM, suggesting that the
309 relationship with temperatures (both ambient air and enclosure) is not linear. Thus, a second
310 model (model 2) was built using the enclosure temperature as a polynomial function. The best
311 results were found by using a polynomial of second order (Table 1). Model diagnostics indicated
312 a further improvement with respect to model 1 (adjusted $r^2=0.90$, RMSE=4.4 ppb and partial F-
313 test $p < 0.001$). Model 2 also exhibited an improvement of the fit of weekly-averaged data (Figure
314 2) and a non-statistically significant Theil-Sen slope ($p > 0.1$). This latter result confirms that
315 model 2 successfully corrected the negative effects of temperature on the GSS sensors. Therefore,
316 this model represents a useful, easy way to correct data measured with GSS sensors to return
317 “FRM-like” ozone concentrations by including two variables easily measurable (or available
318 from existing monitoring networks).

319 Another model (model 3) was tested by adding NO₂ to model 2. Despite results
320 indicating an improvement in the goodness of fit with respect to model 2 (adjusted $r^2=0.91$,
321 RMSE=4.2 ppb and partial F-test $p<0.001$), model 3 also exhibited higher RMSE of the hourly-
322 and weekly-averaged data (Figure 2) and a slight increase of the Theil-Sen slope (Figure S7).
323 Model 3 results showed larger differences during weekends (particularly on Sundays) that are
324 likely related to the decreased NO₂ concentrations with the lower road traffic emissions. It also
325 confirms the work of Lin *et al.* (2015) showing that NO₂ had only a limited effect on the O₃
326 sensor.

328 **3.6 Viability of proposed models**

329 The main purpose in using low-cost monitors is to increase the spatial resolution of
330 routine monitoring networks by deploying a larger number of sites. Since individual sensors may
331 vary in performances, the 10 monitors were co-located under lab conditions and exposed to
332 different O₃ concentrations (<5, 50, and 100 ppb). The inter-monitor Pearson correlation
333 coefficients ranged from 0.97 to 0.99, indicating a very good agreement among the monitors.
334 This result allows applying the proposed correction models to the multiple monitors deployed at
335 locations other than where an FEM monitor is deployed.

336 A potential limitation of the study is the deployment of monitors over only 4 months in
337 summer/early fall weather conditions. The ambient air temperatures recorded throughout the
338 sampling campaign varied between 0°C and 38°C, allowing the extension of correction models
339 over the sensor's operating temperature range (0°C to 40°C). The deployment of these GSS
340 sensors outdoors under colder weather conditions would likely be possible when the monitors are
341 placed in a warmed enclosure (e.g. using a small light bulb for heating). However, a careful
342 evaluation of the validity of the proposed correction under such conditions must be performed.

344 **4 Conclusions**

345 The poor and sparse spatial coverage of current air quality monitoring networks in the
346 U.S. limits the assessment of exposure to O₃ in epidemiological studies. Limited predictive
347 accuracy may lead to potential exposure misclassification resulting in negatively biased health
348 effect estimates. This study demonstrate that the Aeroqual Series 500 monitors coupled with O₃
349 semiconductor oxide sensors could provide improved spatial coverage in routine monitoring

350 networks. However, a careful calibration must be performed prior their deployment to check or
351 adjust the original calibration. The monitor worked well over 4 months with no problems. The
352 raw field data showed a ~12% overestimation bias with respect to data measured under clean
353 laboratory air conditions. The application of correction models including the temperature in the
354 monitor enclosure and ambient RH was able to produce “FRM-like” ozone concentrations
355 explaining 90% of the variance.

356

357 **ACKNOWLEDGEMENTS**

358 This work was funded by the National Institute of Environmental Health Sciences (Grant #P30
359 ES001247). The authors gratefully acknowledge (i) the New York State Department of
360 Environmental Conservation for providing the air quality data measured at the ROC site; (ii)
361 NOAA National Climatic Data Center for providing weather data; and (iii) NOAA/OAR/ESRL
362 PSD, Boulder, Colorado, USA for providing NCEP Reanalysis data from their Web site at
363 <https://www.esrl.noaa.gov/psd/>.

364

365 **REFERENCES**

- 366 Aeroqual (2018). Aeroqual Series 200/300/500 User Guide. Aeroqual Ltd. Auckland, New
367 Zealand. Available at: [https://d2pwrxb99jwry6.cloudfront.net/wp-](https://d2pwrxb99jwry6.cloudfront.net/wp-content/uploads/Environmental-factors-in-the-operation-of-GSS-ozone-sensors.pdf)
368 [content/uploads/Environmental-factors-in-the-operation-of-GSS-ozone-sensors.pdf](https://d2pwrxb99jwry6.cloudfront.net/wp-content/uploads/Environmental-factors-in-the-operation-of-GSS-ozone-sensors.pdf) (last
369 accessed January 2018)
- 370 Ainsworth, E.A., Yendrek, C.R., Sitch, S., Collins, W.J. and Emberson, L.D. (2012). The effects
371 of tropospheric ozone on net primary productivity and implications for climate change.
372 *Annu. Rev. Plant Biol.*, 63: 637-661.
- 373 Aliwell, S.R., Halsall, J.F., Pratt, K.F.E., O'Sullivan, J., Jones, R.L., Cox, R.A., Utembe, S.R.,
374 Hansford, G.M. and Williams, D.E. (2001). Ozone sensors based on WO₃: a model for
375 sensor drift and a measurement correction method. *Meas. Sci. Technol.*, 12: 684-690.
- 376 Bart, M., Williams, D.E., Ainslie, B., McKendry, I., Salmond, J., Grange, S.K., Alavi-Shoshtari,
377 M., Steyn, D. and Henshaw, G.S. (2014). High density ozone monitoring using gas
378 sensitive semi-conductor sensors in the Lower Fraser Valley, British Columbia. *Environ.*
379 *Sci. Technol.*, 48: 3970-3977.
- 380 Bell, M.L., Zanobetti, A. and Dominici, F. (2014). Who is more affected by ozone pollution? A
381 systematic review and meta-analysis. *Am. J. Epidemiol.*, 180: 15-28.
- 382 Carslaw, D.C., Beevers, S.D., Ropkins, K. and Bell, M.C. (2006). Detecting and quantifying
383 aircraft and other on-airport contributions to ambient nitrogen oxides in the vicinity of a
384 large international airport. *Atmos. Environ.*, 40: 5424-5434.
- 385 Cooper, O.R., Parrish, D.D., Ziemke, J., Balashov, N.V., Cupeiro, M., Galbally, I.E., Gilge, S.,
386 Horowitz, L., Jensen, N.R., Lamarque, J.F. and Naik, V. (2014). Global distribution and

387 trends of tropospheric ozone: An observation-based review. *Elementa*, 2: 000029, doi:
388 10.12952/journal.elementa.000029

389 Emami, F., Masiol, M. and Hopke, P.K. (2018). Air pollution at Rochester, NY: Long-term
390 trends and multivariate analysis of upwind SO₂ source impacts. *Sci. Total Environ.*, 612:
391 1506-1515.

392 Fowler, D., Pilegaard, K., Sutton, M.A., Ambus, P., Raivonen, M., Duyzer, J., Simpson, D.,
393 Fagerli, H., Fuzzi, S., Schjørring, J.K. and Granier, C. (2009). Atmospheric composition
394 change: ecosystems–atmosphere interactions. *Atmos. Environ.*, 43: 5193-5267.

395 Grange, S.K., Carslaw, D.C. and Lewis, A.C. (2016). Source apportionment advances with
396 bivariate polar plots, correlation, and regression techniques. *Atmos. Environ.* 145: 128-
397 134.

398 Jerrett, M., Burnett, R.T., Pope III, C.A., Ito, K., Thurston, G., Krewski, D., Shi, Y., Calle, E.
399 and Thun, M. (2009). Long-term ozone exposure and mortality. *N. Engl. J. Med.*, 360:
400 1085-1095.

401 Kumar, P., Morawska, L., Martani, C., Biskos, G., Neophytou, M., Di Sabatino, S., Bell, M.,
402 Norford, L. and Britter, R. (2015). The rise of low-cost sensing for managing air
403 pollution in cities. *Environ. Int.*, 75: 199-205.

404 Lin, C., Gillespie, J., Schuder, M.D., Duberstein, W., Beverland, I.J. and Heal, M.R. (2015).
405 Evaluation and calibration of Aeroqual series 500 portable gas sensors for accurate
406 measurement of ambient ozone and nitrogen dioxide. *Atmos. Environ.*, 100: 111-116.

407 Mesinger, F., DiMego, G., Kalnay, E., Mitchell, K., Shafran, P.C., Ebisuzaki, W., Jović, D.,
408 Woollen, J., Rogers, E., Berbery, E.H. and Ek, M.B. (2006). North American regional
409 reanalysis. *Bull. Am. Meteorol. Soc.*, 87: 343-360.

410 Monks, P.S. (2005). Gas-phase radical chemistry in the troposphere. *Chem. Soc. Rev.*, 34: 376-
411 395.

412 Monks, P.S., Archibald, A.T., Colette, A., Cooper, O., Coyle, M., Derwent, R., Fowler, D.,
413 Granier, C., Law, K.S., Mills, G.E. and Stevenson, D.S. (2015). Tropospheric ozone and
414 its precursors from the urban to the global scale from air quality to short-lived climate
415 forcer. *Atmos. Chem. Phys.*, 15: 8889-8973.

416 NYSDEC (New York State Department of Environmental Conservation) (2017). 2017 Annual
417 Monitoring Network Plan, New York State Ambient Air Monitoring Program. Bureau of
418 Air Quality Surveillance, NYSDEC, Albany, NY,
419 http://www.dec.ny.gov/docs/air_pdf/2017plan.pdf, Last access: 20 January 2018.

420 Palmer, P.I., Jacob, D.J., Fiore, A.M., Martin, R.V., Chance, K. and Kurosu, T.P. (2003).
421 Mapping isoprene emissions over North America using formaldehyde column
422 observations from space. *J. Geophys. Res.-Atmos.*, 108: 4180,
423 doi:10.1029/2002JD002153.

424 Seinfeld, J.H. and Pandis, S.N. (2016). *Atmospheric Chemistry and Physics: From Air Pollution*
425 *to Climate Change*, John Wiley & Sons, Hoboken, NJ.

426 Sen, P.K. (1968). Estimates of regression coefficient based on Kendall's tau. *J. Am. Stat. Assoc.*,
427 63: 1379-1389.

428 Sindelarova, K., Granier, C., Bouarar, I., Guenther, A., Tilmes, S., Stavrou, T., Müller, J.F.,
429 Kuhn, U., Stefani, P. and Knorr, W. (2014). Global data set of biogenic VOC emissions
430 calculated by the MEGAN model over the last 30 years. *Atmos. Chem. Phys.*, 14: 9317-
431 9341.

432 Snyder, E.G., Watkins, T.H., Solomon, P.A., Thoma, E.D., Williams, R.W., Hagler, G.S.,
433 Shelow, D., Hindin, D.A., Kilaru, V.J., and Preuss, P.W. (2013). The changing paradigm
434 of air pollution monitoring. *Environ. Sci. Technol.*, 47: 11369–11377.

435 Stevenson, D.S., Young, P.J., Naik, V., Lamarque, J.F., Shindell, D.T., Voulgarakis, A., Skeie,
436 R.B., Dalsoren, S.B., Myhre, G., Bernsten, T.K., and Folberth, G.A. (2013). Tropospheric
437 ozone changes, radiative forcing and attribution to emissions in the Atmospheric
438 Chemistry and Climate Model Intercomparison Project (ACCMIP). *Atmos. Chem. Phys.*,
439 13: 3063-3085.

440 Theil, H. (1950). A rank invariant method of linear and polynomial regression analysis, i, ii, iii.
441 *Proc. Konink. Nederl. Akad. Wetensch. A.*, 53: 386-392, 521-525, 1397-1412.

442 Turner, M.C., Jerrett, M., Pope III, C.A., Krewski, D., Gapstur, S.M., Diver, W.R., Beckerman,
443 B.S., Marshall, J.D., Su, J., Crouse, D.L. and Burnett, R.T. (2016). Long-term ozone
444 exposure and mortality in a large prospective study. *Am. J. Respir. Crit. Care Med.*, 193:
445 1134-1142.

446 Uria-Tellaetxe, I., and Carslaw D.C. (2014). Source identification using a conditional bivariate
447 Probability function. *Environ. Mod. Softw.*, 59: 1-9.

448 USEPA (United States Environmental Protection Agency) (2013). Transfer Standards For
449 Calibration of Air Monitoring Analyzers for Ozone, Technical Assistance Document,
450 Report No. EPA ~~0541-B-13-004~~ Quality Planning and Standards, Air
451 Quality Assessment Division,
452 <https://www3.epa.gov/ttnamti1/files/ambient/qaqc/OzoneTransferStandardGuidance.pdf>,
453 Last access: 8 February, 2018.

454 USEPA (United States Environmental Protection Agency) (2017). List of Designated Reference
455 and Equivalent Methods, Issue of June 16, 2017, USEPA National Exposure Research
456 Laboratory, Triangle Park, NC. <https://www3.epa.gov/ttn/amtic/criteria.html>, Last
457 access: 22 January 2018.

458 White, R.M., Paprotny, I., Doering, F., Cascio, W.E., Solomon, P.A. and Gundel, L.A. (2012).
459 Sensors and 'apps' for community-based: Atmospheric monitoring. *EM: Air and Waste
460 Management Association's Magazine for Environmental Managers*, (MAY), 36-40.

461 Williams, D.E., Henshaw, G.S., Wells, D.B., Ding, G., Wagner, J., Wright, B.E., Yung, Y.F. and
462 Salmond, J.A. (2009). Development of low-cost ozone measurement instruments
463 suitable for use in an air quality monitoring network. *Chem. New Zealand*, 73: 27–33

464 Williams, D.E., Henshaw, G.S., Bart, M., Laing, G., Wagner, J., Naisbitt, S. and Salmond, J.A.
465 (2013). Validation of low-cost ozone measurement instruments suitable for use in an air-
466 quality monitoring network. *Meas. Sci. Technol.*, 24: 065803.

467 TABLES

468

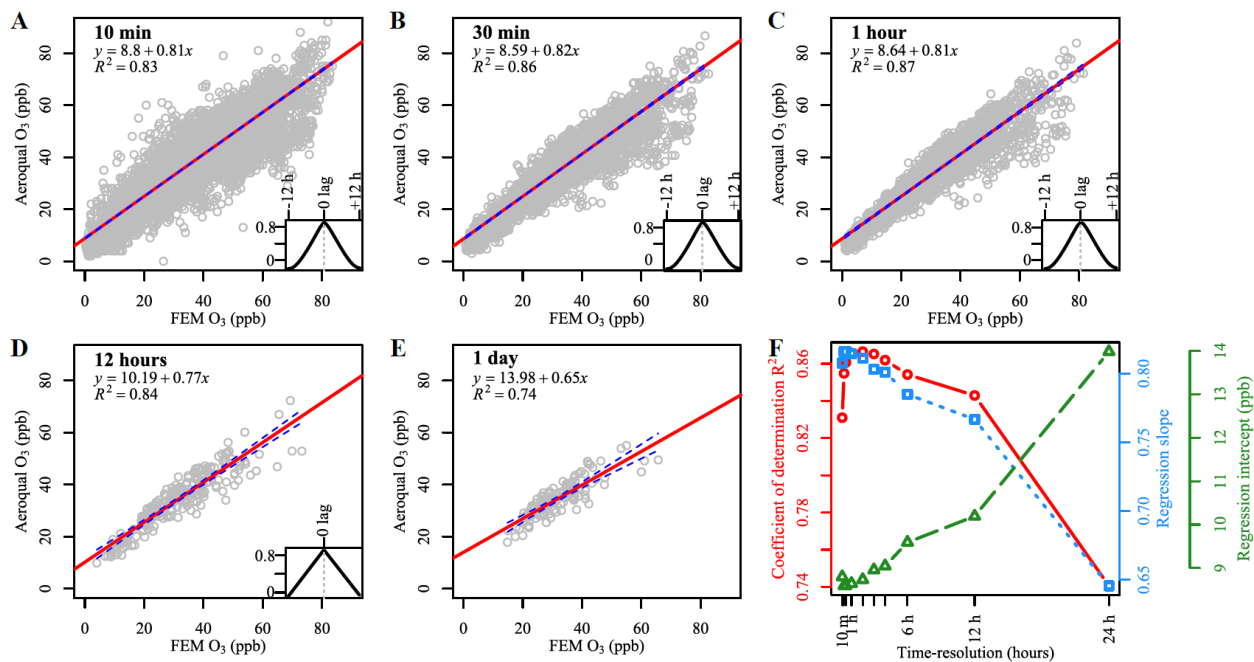
469 **Table 1.** Results of the regressions analyses to return “FEM-like” Aeroqual concentrations.

470

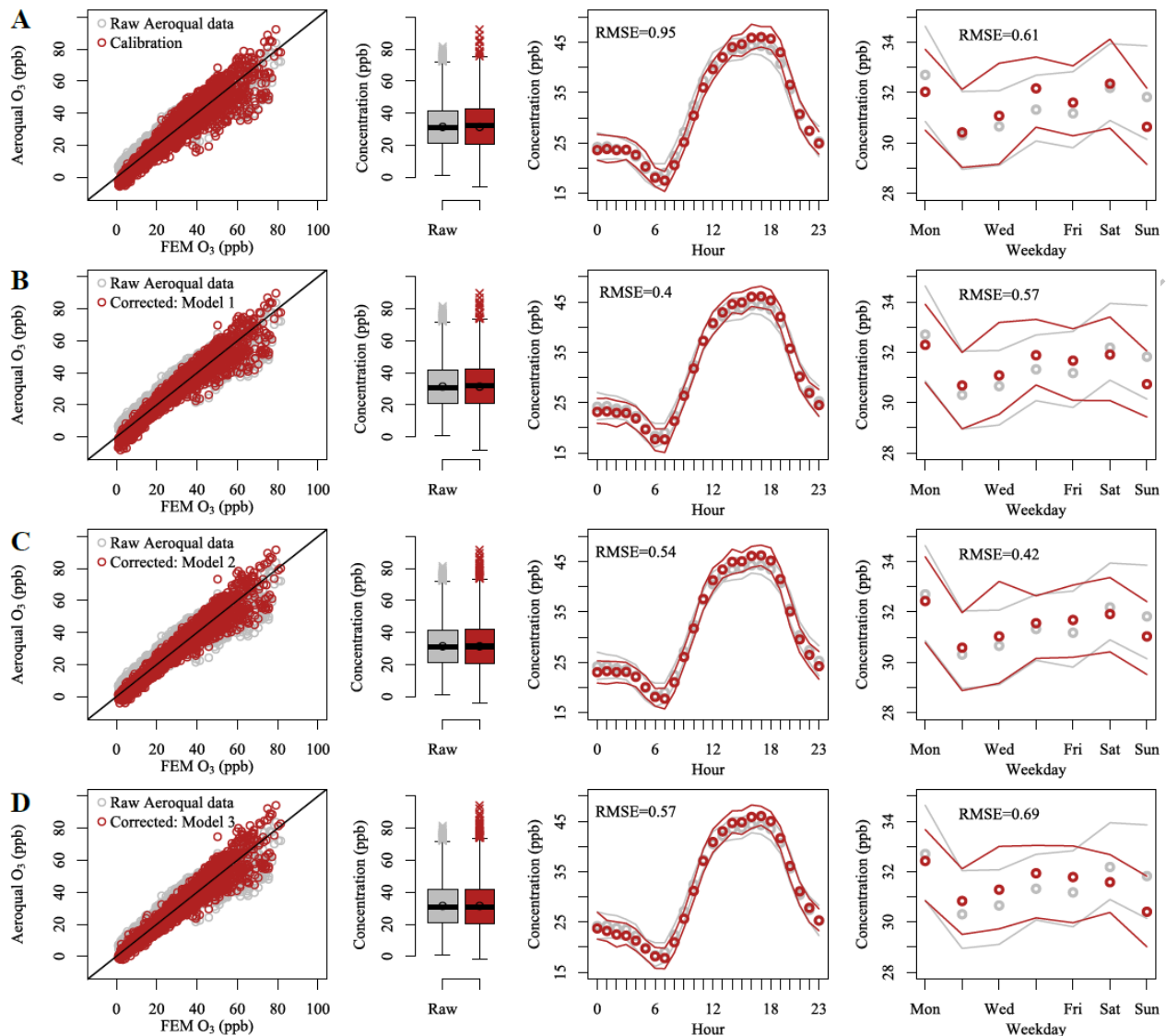
Selected model	Coefficients and estimators				
	Unit	Estimate	Std. error	t value	p
Calibration: Aeroqual= $\beta_0+(\beta_1 \cdot \text{FEM})$					
R ²	—	0.87	—	—	—
β_0	ppb	8.64	0.211806	40.8	<0.001
β_1	ppb	0.81	0.006041	134.8	<0.001
RMSE	ppb	5.0	—	—	—
MAE	ppb	3.9	—	—	—
Model 1: Aeroqual= $\beta_0+(\beta_1 \cdot \text{FEM})+(\beta_2 \cdot \text{Encl. Temp.})+(\beta_3 \cdot \text{RH})$					
R ²	—	0.89	—	—	—
R _{adj} ²	—	0.89	—	—	—
β_0	ppb	20.139	0.771	26.1	<0.001
β_1	ppb	0.912	0.009	105.6	<0.001
β_2	°C	-0.476	0.021	-22.4	<0.001
β_3	%	-0.059	0.006	-9.4	<0.001
RMSE	ppb	4.6	—	—	—
MAE	ppb	3.5	—	—	—
Model 2: Aeroqual= $\beta_0+(\beta_1 \cdot \text{FEM})+(\beta_2 \cdot \text{Encl. Temp.})+(\beta_3 \cdot \text{Encl. Temp.}^2)+(\beta_4 \cdot \text{RH})$					
R ²	—	0.90	—	—	—
R _{adj} ²	—	0.90	—	—	—
β_0	ppb	11.730	0.901	13.0	<0.001
β_1	ppb	0.925	0.008	111.5	<0.001
β_2	°C	0.536	0.066	8.2	<0.001
β_3	°C	-0.025	0.002	-16.2	<0.001
β_4	%	-0.079	0.006	-12.8	<0.001
RMSE	ppb	4.4	—	—	—
MAE	ppb	3.4	—	—	—
Model 3: Aeroqual= $\beta_0+(\beta_1 \cdot \text{FEM})+(\beta_2 \cdot \text{Encl. Temp.})+(\beta_3 \cdot \text{Encl. Temp.}^2)+(\beta_4 \cdot \text{RH})+(\beta_5 \cdot \text{NO}_2)$					
R ²	—	0.91	—	—	—
R _{adj} ²	—	0.91	—	—	—
β_0	ppb	13.953	0.865	16.1	<0.001
β_1	ppb	0.875	0.008	104.3	<0.001
β_2	°C	0.516	0.062	8.3	<0.001
β_3	°C	-0.023	0.001	-16.1	<0.001
β_4	%	-0.061	0.006	-10.2	<0.001
β_5	ppb	-0.415	0.024	-17.5	<0.001
RMSE	ppb	4.2	—	—	—
MAE	ppb	3.1	—	—	—

471

472 FIGURES
473



474
475 **Figure 1.** Linear regression of Aeroqual O₃ vs. FEM O₃ at varying time resolutions (a: 10 min;
476 b:30 min; c: 1 h; d: 12 h; e: 24 h), and changes in the regression coefficients (f). The regression
477 line is solid and red colored; the 95th confidence intervals are drawn in dashed blue. The
478 regression plots (a-e) also report the cross-correlation curves (bottom-right).



479
 480 **Figure 2.** Results of the application of calibration and corrections. Each row of plots corresponds to a model, as in Table 1: calibration (A) and linear models (B= model 1, C= model 2, D= model 3). The scatterplots on the left show the fit of 1 h-averaged data with FEM (black lines represent the 1:1 relationship). The boxplots show the distribution of raw (grey) and corrected (red) data. Lines represent the medians, boxes are the 25-75th percentile ranges, whiskers show ± 1.5 interquartile ranges, circles are the arithmetic means. The plots on the right show the diurnal and weekly patterns of raw (grey) and corrected (red) data. Circles represent the averages, lines draw the 95th confidence intervals of the averages computed by bootstrapping the data ($n=2000$). RMSE are also reported for comparing the goodness of the fits.